Featured in Physics

Two-Dimensional Supersolid Formation in Dipolar Condensates

T. Bland,[1] E. Poli,[2] C. Politi,[1,2] L. Klaus,[1,2] M. A. Norcia,[1] F. Ferlaino,[1,2] L. Santos,[3] and R. N. Bisset[2,*]
[1]Institut für Quantenoptik und Quanteninformation, Österreichische Akademie der Wissenschaften, Innsbruck 6020, Austria
[2]Institut für Experimentalphysik, Universität Innsbruck, Innsbruck 6020, Austria
[3]Institut für Theoretische Physik, Leibniz Universität Hannover, Hannover 30167, Germany

(Received 14 July 2021; revised 19 January 2022; accepted 11 April 2022; published 13 May 2022)

Dipolar condensates have recently been coaxed to form the long-sought supersolid phase. While one-dimensional supersolids may be prepared by triggering a roton instability, we find that such a procedure in two dimensions (2D) leads to a loss of both global phase coherence and crystalline order. Unlike in 1D, the 2D roton modes have little in common with the supersolid configuration. We develop a finite-temperature stochastic Gross-Pitaevskii theory that includes beyond-mean-field effects to explore the formation process in 2D and find that evaporative cooling directly into the supersolid phase—hence bypassing the first-order roton instability—can produce a robust supersolid in a circular trap. Importantly, the resulting supersolid is stable at the final nonzero temperature. We then experimentally produce a 2D supersolid in a near-circular trap through such an evaporative procedure. Our work provides insight into the process of supersolid formation in 2D and defines a realistic path to the formation of large two-dimensional supersolid arrays.

DOI: 10.1103/PhysRevLett.128.195302

The supersolid phase was predicted to simultaneously exhibit crystalline order and superfluidity [1–6]. While it remains elusive in helium, recent developments in ultracold quantum gases have finally made supersolidity a reality, providing an excellent platform for the control and observation of these states. Important early advances were made in systems with spin-orbit coupling [7,8] and cavity-mediated interactions [9], where supersolid properties were observed in rigid crystal configurations. Bose-Einstein condensates (BECs) with dipole-dipole interactions have now been observed in a supersolid state with deformable crystals [10–13], with their lattices genuinely arising from the atom-atom interactions [14–16].

In the first dipolar supersolid experiments, translational symmetry was broken only along one axis, giving rise to a one-dimensional (1D) density wave, commonly referred to as a 1D droplet array [10–12]. A more recent experiment has created the first states with two-dimensional (2D) supersolidity in elongated traps of variable aspect ratio [13]. This opens the door to study vortices and persistent currents [17–20], as well as exotic ground state phases predicted for large atom numbers [21–24].

It is still an open question whether 2D arrays provide as favorable conditions for supersolidity as 1D arrays do. In 1D, following an interaction quench from an unmodulated to modulated BEC, the density pattern induced by a roton instability [14,25–28] can smoothly connect with the final supersolid array [10–12]. This transition, hence, has a weakly first-order character or is even continuous [29,30], and such quenches through the transition cause only small excitations of the resulting supersolid [10–12]. While it has been predicted that a similar procedure may lead to coherence between three droplets in a triangular configuration [31], earlier work with nondipolar superfluids suggests that such symmetry-breaking quenches may be unfavorable for supersolid formation in 2D and 3D [32,33].

An alternative method exists to experimentally produce dipolar supersolids. Instead of quenching the interactions to trigger a roton instability, it is possible to cool a thermal sample directly into the supersolid state using evaporative cooling techniques [12,34]. Crucially, this is the only known method for producing 2D supersolids to date [13]. While a dynamic interaction quench may be described by the extended Gross-Pitaevskii equation (eGPE) [35–38], we are not aware of any available theory to model the required evaporation process. From a theoretical perspective, much remains unknown about evaporative supersolid formation. Is it a general feature that the droplets form before global phase coherence develops, as reported in Ref. [34]? Under what conditions do defects persist? Such answers will be paramount in the quest for ever-larger 2D supersolids, as well as for the observation of vortices embedded within them.

In this Letter, we explore the formation of large 2D supersolids in circular-shaped traps. We develop a finite-temperature Stochastic eGPE (SeGPE) theory to model the entire evaporative cooling process. Importantly, our theory includes the beyond-mean-field quantum fluctuations responsible for stabilizing the individual droplets.

We compare the evaporative cooling formation dynamics with those resulting from an interaction quench, finding striking differences between the two protocols. Following

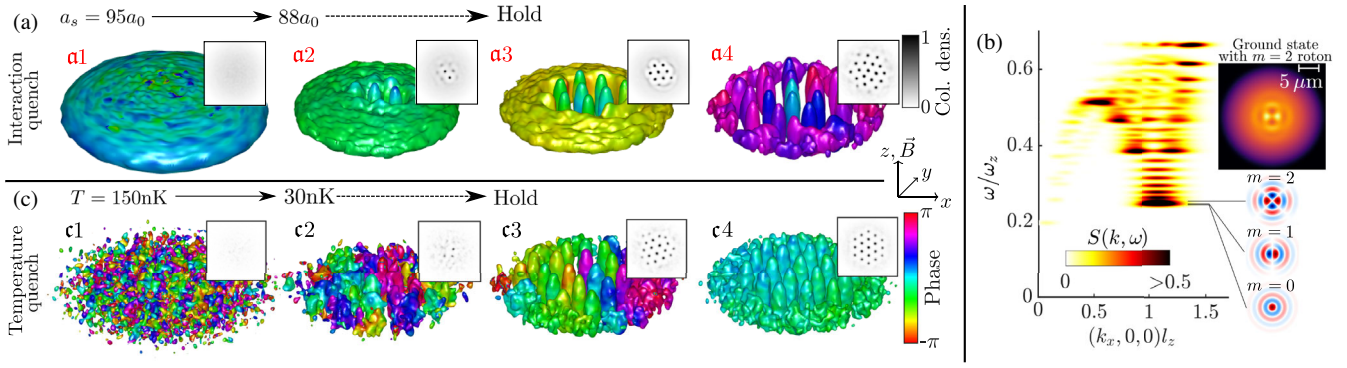

FIG. 1. (a) Crystal preparation from interaction quench, evolved with the eGPE, for $N \approx 2.1 \times 10^5$ Dy atoms [quench (i)]. Isosurfaces are at 5% max density, with color indicating phase. Insets: z column densities normalized to max value from the entire simulation. (b) Dynamic structure factor for an unmodulated BEC ($a_s = 92a_0$) in energy-momentum space, normalized to peak value. The lowest-energy roton modes are indicated, and the ground state with an $m = 2$ roton mode added is shown, revealing the localized nature of the rotons. Parameters are otherwise the same as in (a). (c) Crystal preparation from temperature quench (evaporative cooling) evolved with the SeGPE [quench (ii)]. The temperature decreases as the chemical potential and condensate number rise, with scattering length fixed at $a_s = 88a_0$. For all subplots $f_{x,y,z} = (33, 33, 167)$ Hz, and $l_z = \sqrt{\hbar/m\omega_z}$.

an interaction quench, the 2D crystal grows nonlinearly with the droplets developing sequentially, producing configurations that are unrelated to any roton mode combination of the original unmodulated BEC. The resulting crystal is substantially excited and lacks global phase coherence. Alternatively, by directly cooling into the supersolid regime, our SeGPE theory predicts the formation of large 2D supersolids in circular traps, with global phase coherence that remains robust at finite temperature. To benchmark our theory—as well as to test the direct cooling protocol for pancake-shaped trapping geometries—we perform experiments and observe a 7-droplet hexagonal supersolid in a near-circular trap.

Formalism.—We are interested in ultracold, dipolar Bose gases harmonically confined in 3D with trapping frequencies $\omega_{x,y,z} = 2\pi f_{x,y,z}$. Two-body contact interactions and the long-ranged, anisotropic dipole-dipole interactions are well described by a pseudopotential, $U(\mathbf{r}) = (4\pi\hbar^2 a_s/m)\delta(\mathbf{r}) + (3\hbar^2 a_{\rm dd}/m)[(1 - 3\cos^2\theta)/r^3]$, with a_s being the s-wave scattering length and $a_{\rm dd} = \mu_0\mu_m^2 m/12\pi\hbar^2$ the dipole length, with magnetic moment μ_m, and θ is the angle between the polarization axis (z axis) and the vector joining two particles. The ratio $\epsilon_{\rm dd} = a_{\rm dd}/a_s$ (for $a_s > 0$) is convenient to keep in mind, since for $\epsilon_{\rm dd} \leq 1$ the ground state will be an unmodulated BEC, whereas for the dipole-dominated regime $\epsilon_{\rm dd} > 1$ the unmodulated BEC may become unstable [39]. Here, we always consider ^{164}Dy, with $a_{\rm dd} = 131a_0$. The eGPE has been described elsewhere [35–38], and its details have been deferred to Supplemental Material [40].

We phenomenologically introduce a finite-temperature simple growth SeGPE theory [55]. This describes the "classical" field, $\Psi(\mathbf{r}, t)$, of all highly populated modes up to an energy cutoff. The dynamics are governed by [56]

$$i\hbar\frac{\partial\Psi}{\partial t} = \hat{\mathcal{P}}\{(1 - i\gamma)(\mathcal{L}[\Psi] - \mu)\Psi + \eta\}. \tag{1}$$

Here, $\mathcal{L}$ is the eGPE operator defined in Ref. [40], and γ describes the coupling of the classical field modes to the high-lying modes. We find that $\gamma = 7.5 \times 10^{-3}$ gives good agreement to the condensate number growth rate of a recent experiment under comparable conditions [34] (see also Ref. [40]). The dynamical noise term η, subject to noise correlations given by $\langle\eta^*(\mathbf{r}, t)\eta(\mathbf{r}', t')\rangle = 2\hbar\gamma k_B T\delta(t - t')\delta(\mathbf{r} - \mathbf{r}')$, means that each simulation run is unique. Finally, $\hat{\mathcal{P}}$ is a projector which constrains the dynamics of the system up to energy cutoff $\epsilon_{\rm cut}(\mu) = 2\mu$—consistent with previous treatments [57,58]—where we use the final μ after evaporative cooling.

Supersolid formation simulations.—With these two theories in hand, we perform two kinds of dynamic quench simulations in a pancake-shaped trap, where in both cases the ground state for the final parameters would be a 19-droplet supersolid:

(i) An interaction quench from an unmodulated BEC to the supersolid regime using the eGPE [Fig. 1(a)]. Noise is first added to the BEC ground state [59], and this is evolved for a 20 ms equilibration time before the interaction strength is linearly ramped over the next 30 ms from $a_s = 95a_0$ to $a_s = 88a_0$—crossing the roton phase transition to the supersolid regime—and then held constant again for the remainder of the simulation.

(ii) A temperature quench from a thermal cloud to the supersolid phase using the SeGPE [Fig. 1(c)]. Each simulation begins with a 200 ms equilibration time at fixed high temperature $T = 150$ nK to generate a thermal cloud. To simulate the evaporative cooling process, the chemical potential and temperature are then linearly ramped over 100 ms, from $(\mu, T) = (-12.64\hbar\omega_z, 150\ \text{nK})$ to

$(12.64\hbar\omega_z, 30\ \mathrm{nK})$, mimicking the growing condensate number observed in experiments [60,61], while the scattering length is always held fixed at $a_s = 88a_0$.

Focusing first on the interaction quench, the density isosurfaces in Fig. 1(a) represent snapshots at various times for a single simulation run, revealing intriguing formation dynamics. Initial droplets are seeded through unstable roton modes, but staggered droplet formation reveals a process of *nonlinear crystal growth*, as highlighted by the column densities shown as insets in Fig. 1(a). In Fig. 1(a2), two central droplets have already attained their final peak density, while a secondary ring of droplets is only just beginning to form. Then, in Fig. 1(a3), eight droplets have fully matured, and the process continues radially outward until a 19-droplet crystal is approximately attained. Similar droplet formation dynamics have been predicted in optical media [62].

The colors on the density isosurfaces in Fig. 1(a) represent the wave function phase. The color scale is recentered in each subplot, and an ideal phase coherent solution would have a uniform color everywhere. Importantly, the crystal growth process disrupts the global phase coherence, as evidenced by the various colors in Fig. 1(a4), leaving an excited crystal in which some outer droplets dissolve and reemerge from the halo. Note that the situation does not qualitatively change for reduced initial noise or gentler interaction ramps, suggesting that the strong excitations result from a first-order character of the roton instability in 2D.

We explain the interaction quench dynamics by calculating the elementary excitations of the unmodulated BEC close to the roton instability, i.e., for $a_s = 92a_0$. These results are displayed in Fig. 1(b) as the dynamic structure factor $S(\mathbf{k}, \omega)$, which predicts the system response to perturbations of momentum $\hbar\mathbf{k}$ and energy $\hbar\omega$ [28,63–65] (also see Ref. [40]). A roton minimum can be seen at $k_x l_z \approx 1.1$, and we plot the lowest roton modes corresponding to $m = 0$, 1, 2, with m being the angular quantum number in the z direction [66]. On the top right is the density obtained by adding an $m = 2$ roton mode to the BEC wave function, revealing how rotons are confined to high-density regions [67,68]. This reveals a qualitative difference between the 1D and 2D situations, since, from a simple geometric standpoint, in 2D the high-density region inherently encompasses a smaller proportion of the total atom number. Thus, the roton-induced droplet number is only a small fraction of the final droplet number, meaning the droplets appear sequentially for 2D.

Another qualitative difference between 1D and 2D is a kind of frustration. First, note that our target supersolid ground state for the final quench parameters is a 19-droplet crystal, with a central droplet [see the inset of Fig. 2(b)]. Only an $m = 0$ roton mode [see Fig. 1(b)] could directly trigger the formation of a central droplet, but then only concentric rings could form further out. Thus, unlike for 1D, no single roton mode can smoothly connect the unmodulated BEC to the 2D supersolid ground state.

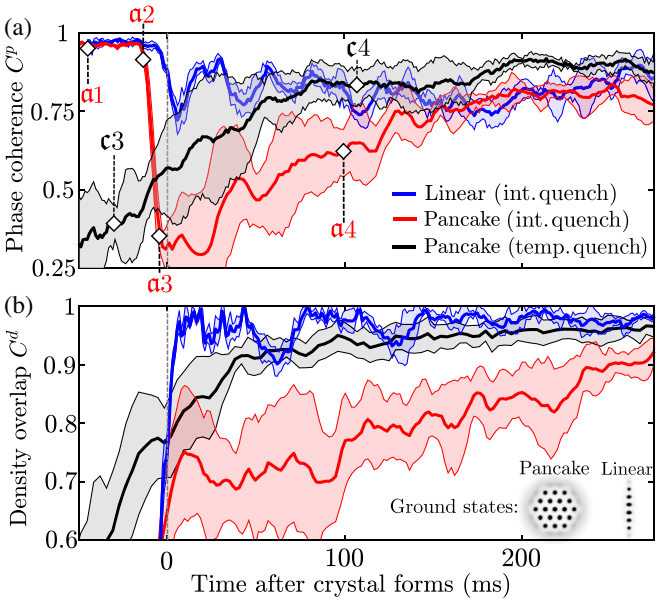

FIG. 2. Supersolid quality. (a) Global phase coherence C^p over time for interaction quenches [quench (i)] into linear chain (blue) and pancake crystal (red) and temperature quenches [quench (ii)] into the pancake crystal (black). Diamonds link to example frames in Figs. 1(a) and 1(c). Each curve is averaged over 3–5 runs with an error band marking one standard deviation. Time $t = 0$ corresponds to when the crystals first fully mature. (b) Density overlap C^d between the time-dependent and ground state densities. Parameters are the same as Fig. 1, but for linear chain $f_{x,y,z} = (33, 110, 167)$ Hz and $N = 82 \times 10^3$.

Next, we analyze the finite-temperature quench results. Figure 1(c) shows snapshots of the condensate growth, demonstrating that both the crystal structure and the global phase coherence—evidenced by the uniform color in Fig. 1(c4)—develop soon after the quench. Note that timescales will be quantified shortly. It is also an important result in itself that we predict such a large 2D supersolid to be stable against thermal fluctuations (recall that $T_{\mathrm{final}} = 30$ nK). As they form, each droplet individually has a uniform phase that may be different from that of its neighbors, sometimes creating vortex pairs between droplets of different phase. In this scenario, the droplets do not form as a result of a roton instability, and the partial phase coherence continues to improve after the crystal has formed, consistent with earlier observations [34]. Occasionally, long-lived isolated vortices remain near the center of the supersolid. Simulation videos are provided in Supplemental Material [40].

Supersolid quality.—We seek to quantify the resulting supersolid quality for both quench protocols. We start by analyzing the phase excitations, taking the phase coherence C^p with a similar measure presented in Ref. [10]. A value of $C^p = 1(0)$ implies global phase

coherence (incoherence) [69]. In Fig. 2(a), we plot this quantity for interaction quenches into the pancake supersolid regime (red) and linear supersolid regime (blue) and temperature quenches into the pancake supersolid (black). The time $t = 0$ indicates when the droplet number has approximately stabilized and the crystal has first matured [70]. For the linear chain, the system remains coherent (high $C^p \approx 0.8$), indicating a stable supersolid. However, quenching into the pancake geometry is qualitatively different, with strong incoherence ($C^p \approx 0.3$) soon after crystal formation, recovering a high value at around 150 ms after the crystal forms. During evaporative cooling, the global phase coherence is predicted by the high value of $C^p \approx 0.8$ around 50 ms after the crystal forms, with qualitatively similar values to the interaction quench simulations for the linear supersolid case.

We quantify the quality of the supersolid crystal by measuring the density overlap C^d between the ground state target solution and the time-dependent wave function [71]. We find the maximal value of C^d after applying translations and rotations to the state, noting that perfect overlap would give $C^d = 1$. In Fig. 2(b), this quantity is presented for the two geometries, with the ground state solutions shown as insets. For the linear chain, once the droplets have formed, the density overlap rapidly attains $C^d > 0.9$ and remains there, consistent with the interaction quenched state being close to the ground state supersolid. However, the pancake case shows weak overlap after the droplets are formed, which only recovers slowly—after around 300 ms—to values comparable with the linear chain. Primarily, this is due to the sensitivity of droplet positions of C^d and indicates that there are many excited supersolid modes present after the droplets form [40]. Direct evaporative cooling for the pancake case, however, shows that after the droplets have formed they rapidly settle into the expected crystal pattern ($C^d \approx 0.95$).

Finally, it is important to note that for the pancake interaction quench, while the phase coherence is restored by around $t = 150$ ms after the droplets are formed, the crystal remains highly excited until around 300 ms. On these timescales, three-body losses become significant, and it is unlikely that a large supersolid would be observed. In contrast, direct evaporative cooling may lead to a robust supersolid within around 50 ms of the crystal first appearing, a timescale that we find to be weakly dependent on the value of γ [40].

Experimental observation.—While experiments have evaporatively cooled directly into the supersolid phase for linear and elongated 2D configurations [12,13,34], this could prove an optimal method in circular traps for avoiding the excitations associated with crossing the roton instability. We confirm this by producing a 7-droplet hexagon supersolid in a near-circular trap, as shown in Fig. 3. The experimental apparatus and procedure is similar to that described previously [13], but new modifications in the optical dipole trap setup have enabled us to tune between anisotropic and round traps. The current optical trap consists of three 1064 nm wavelength trapping beams, each propagating in the plane perpendicular to gravity. Two of the beams, which cross perpendicularly, have approximately 60 μm waists and define the horizontal trapping frequencies. The third, crossing at a roughly 45° angle from the others, has a waist of approximately 18 μm and is rapidly scanned to create a time-averaged light sheet that defines the vertical confinement.

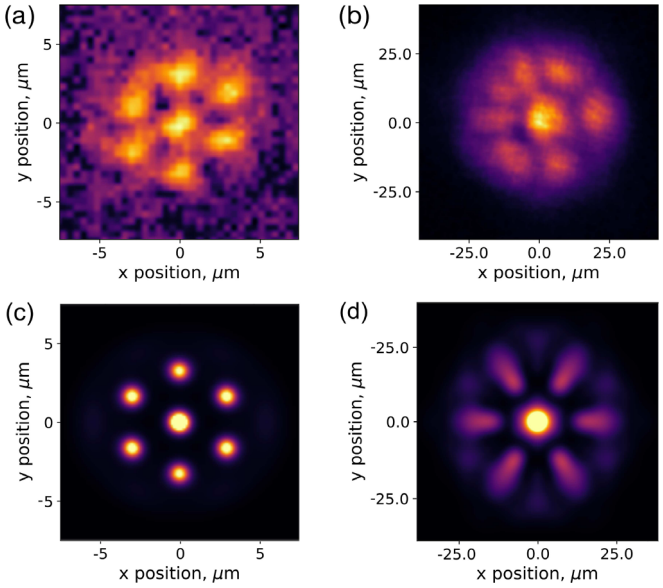

FIG. 3. Experimental realization of a 7-droplet hexagon state. (a) Exemplary *in situ* image of the density profile. (b) Image after 36 ms time-of-flight (TOF) expansion, averaged over 68 trials of the experiment. Hexagonal modulation structure is clearly present in the averaged image. Note the rotation of the hexagon between *in situ* and TOF images. (c),(d) Corresponding simulations for the same trap, and with $a_s = 90a_0$ and $\approx 4.4 \times 10^4$ atoms within the droplets.

In a harmonic trap with frequencies $f_{x,y,z} = [47(1), 43(1), 133(5)]$ Hz, we observe in trap a 7-droplet state consisting of a hexagon with a central droplet, with a condensate atom number of $N \sim 4 \times 10^4$ [Fig. 3(a)]. To confirm that this state is phase coherent, we release the atoms from the trap and image the interference pattern after 36 ms time of flight [Fig. 3(b)]. The presence of clear modulation in the interference pattern averaged over 68 runs of the experiment indicates a well-defined and reproducible relative phase between the droplets and is consistent with our expectations for a phase-coherent state undergoing expansion [Fig. 3(d)], obtained through 3D dynamic simulations starting from the eGPE ground state [Fig. 3(c)]. Even rounder traps are possible, but the slight anisotropy orients the state, helping to observe the reproducible interference pattern.

Summary.—We have theoretically explored the formation of large 2D supersolids using both an interaction

quench from an unmodulated BEC and a temperature quench from a thermal cloud. For the latter, we developed a finite-temperature stochastic Gross-Pitaevskii theory that can simulate evaporative cooling directly into the supersolid regime. Our simulations predict that a temperature quench provides a robust path for creating 2D supersolids in circular traps, and we confirm this experimentally by using this method to create a reproducible hexagonal 7-droplet supersolid.

In contrast, the interaction quench results in highly excited crystals that lack global phase coherence in the period following their formation. Interestingly, droplets appear sequentially rather than simultaneously, with the final crystal structure being unrelated to the roton modes that seeded the instability. This is in contrast to the situation for 1D arrays, where an interaction quench through a roton instability can smoothly connect an unmodulated BEC to the supersolid ground state.

Our finite-temperature theory is broadly applicable for future studies on topics such as formation dynamics, supersolid vortices, improved quench protocols to produce large 2D supersolids, and thermal resilience, as well as dipolar droplets in general.

We thank Manfred Mark and the Innsbruck Erbium team for valuable discussions and thank Péter Juhász for carefully reading the manuscript. We acknowledge R. M. W. van Bijnen for developing the code for our eGPE and BdG simulations. Part of the computational results presented have been achieved using the HPC infrastructure LEO of the University of Innsbruck. The experimental team is financially supported through an ERC Consolidator Grant (RARE, No. 681432), an NFRI grant (MIRARE, No. OAW0600) of the Austrian Academy of Science, and the QuantERA grant MAQS by the Austrian Science Fund FWF No. I4391-N. L. S. and F. F. acknowledge the DFG/FWF (Grant No. FOR 2247/I4317-N36) and a joint-project grant from the FWF (Grant No. I4426, RSF/Russland 2019). L. S. thanks the funding by the Deutsche Forschungsgemeinschaft (DFG, German Research Foundation) under Germany's Excellence Strategy—EXC-2123 QuantumFrontiers—390837967. M. A. N. has received funding as an ESQ postdoctoral fellow from the European Unions Horizon 2020 research and innovation program under the Marie Sklodowska-Curie Grant Agreement No. 801110 and the Austrian Federal Ministry of Education, Science and Research (BMBWF). We also acknowledge the Innsbruck Laser Core Facility, financed by the Austrian Federal Ministry of Science, Research and Economy.

*Corresponding author.
russell.bisset@uibk.ac.at

[1] E. P. Gross, Unified theory of interacting bosons, Phys. Rev. **106**, 161 (1957).
[2] A. Andreev and I. Lifshitz, Quantum theory of defects in crystals, Zh. Eksp. Teor. Fiz. **56**, 2057 (1969) [JETP **29**, 1107 (1969)].
[3] D. Thouless, The flow of a dense superfluid, Ann. Phys. (N.Y.) **52**, 403 (1969).
[4] G. Chester, Speculations on Bose-Einstein condensation and quantum crystals, Phys. Rev. A **2**, 256 (1970).
[5] A. J. Leggett, Can a Solid Be "Superfluid"?, Phys. Rev. Lett. **25**, 1543 (1970).
[6] M. Boninsegni and N. V. Prokof'ev, Colloquium: Supersolids: What and where are they?, Rev. Mod. Phys. **84**, 759 (2012).
[7] J.-R. Li, J. Lee, W. Huang, S. Burchesky, B. Shteynas, F. Ç. Top, A. O. Jamison, and W. Ketterle, A stripe phase with supersolid properties in spin–orbit-coupled Bose–Einstein condensates, Nature (London) **543**, 91 (2017).
[8] T. M. Bersano, J. Hou, S. Mossman, V. Gokhroo, X.-W. Luo, K. Sun, C. Zhang, and P. Engels, Experimental realization of a long-lived striped Bose-Einstein condensate induced by momentum-space hopping, Phys. Rev. A **99**, 051602(R) (2019).
[9] J. Léonard, A. Morales, P. Zupancic, T. Esslinger, and T. Donner, Supersolid formation in a quantum gas breaking a continuous translational symmetry, Nature (London) **543**, 87 (2017).
[10] L. Tanzi, E. Lucioni, F. Famà, J. Catani, A. Fioretti, C. Gabbanini, R. N. Bisset, L. Santos, and G. Modugno, Observation of a Dipolar Quantum Gas with Metastable Supersolid Properties, Phys. Rev. Lett. **122**, 130405 (2019).
[11] F. Böttcher, J.-N. Schmidt, M. Wenzel, J. Hertkorn, M. Guo, T. Langen, and T. Pfau, Transient Supersolid Properties in an Array of Dipolar Quantum Droplets, Phys. Rev. X **9**, 011051 (2019).
[12] L. Chomaz, D. Petter, P. Ilzhöfer, G. Natale, A. Trautmann, C. Politi, G. Durastante, R. M. W. van Bijnen, A. Patscheider, M. Sohmen, M. J. Mark, and F. Ferlaino, Long-Lived and Transient Supersolid Behaviors in Dipolar Quantum Gases, Phys. Rev. X **9**, 021012 (2019).
[13] M. A. Norcia, C. Politi, L. Klaus, E. Poli, M. Sohmen, M. J. Mark, R. N. Bisset, L. Santos, and F. Ferlaino, Two-dimensional supersolidity in a dipolar quantum gas, Nature (London) **596**, 357 (2021).
[14] G. Natale, R. M. W. van Bijnen, A. Patscheider, D. Petter, M. J. Mark, L. Chomaz, and F. Ferlaino, Excitation Spectrum of a Trapped Dipolar Supersolid and Its Experimental Evidence, Phys. Rev. Lett. **123**, 050402 (2019).
[15] L. Tanzi, S. Roccuzzo, E. Lucioni, F. Famà, A. Fioretti, C. Gabbanini, G. Modugno, A. Recati, and S. Stringari, Supersolid symmetry breaking from compressional oscillations in a dipolar quantum gas, Nature (London) **574**, 382 (2019).
[16] M. Guo, F. Böttcher, J. Hertkorn, J.-N. Schmidt, M. Wenzel, H. P. Büchler, T. Langen, and T. Pfau, The low-energy goldstone mode in a trapped dipolar supersolid, Nature (London) **574**, 386 (2019).
[17] A. Gallemí, S. M. Roccuzzo, S. Stringari, and A. Recati, Quantized vortices in dipolar supersolid Bose-Einstein-condensed gases, Phys. Rev. A **102**, 023322 (2020).
[18] S. M. Roccuzzo, A. Gallemí, A. Recati, and S. Stringari, Rotating a Supersolid Dipolar Gas, Phys. Rev. Lett. **124**, 045702 (2020).

[19] M. N. Tengstrand, D. Boholm, R. Sachdeva, J. Bengtsson, and S. M. Reimann, Persistent currents in toroidal dipolar supersolids, Phys. Rev. A **103**, 013313 (2021).
[20] F. Ancilotto, M. Barranco, M. Pi, and L. Reatto, Vortex properties in the extended supersolid phase of dipolar Bose-Einstein condensates, Phys. Rev. A **103**, 033314 (2021).
[21] D. Baillie and P. B. Blakie, Droplet Crystal Ground States of a Dipolar Bose Gas, Phys. Rev. Lett. **121**, 195301 (2018).
[22] Y.-C. Zhang, F. Maucher, and T. Pohl, Supersolidity Around a Critical Point in Dipolar Bose-Einstein Condensates, Phys. Rev. Lett. **123**, 015301 (2019).
[23] Y.-C. Zhang, T. Pohl, and F. Maucher, Phases of supersolids in confined dipolar Bose-Einstein condensates, Phys. Rev. A **104**, 013310 (2021).
[24] J. Hertkorn, J.-N. Schmidt, M. Guo, F. Böttcher, K. S. H. Ng, S. D. Graham, P. Uerlings, T. Langen, M. Zwierlein, and T. Pfau, Pattern formation in quantum ferrofluids: From supersolids to superglasses, Phys. Rev. Research **3**, 033125 (2021).
[25] L. Santos, G. V. Shlyapnikov, and M. Lewenstein, Roton-Maxon Spectrum and Stability of Trapped Dipolar Bose-Einstein Condensates, Phys. Rev. Lett. **90**, 250403 (2003).
[26] S. Giovanazzi and D. H. J. O'Dell, Instabilities and the roton spectrum of a quasi-1d Bose-Einstein condensed gas with dipole-dipole interactions, Eur. Phys. J. D **31**, 439 (2004).
[27] D. Petter, G. Natale, R. M. W. van Bijnen, A. Patscheider, M. J. Mark, L. Chomaz, and F. Ferlaino, Probing the Roton Excitation Spectrum of a Stable Dipolar Bose Gas, Phys. Rev. Lett. **122**, 183401 (2019).
[28] L. Chomaz, R. M. W. van Bijnen, D. Petter, G. Faraoni, S. Baier, J. H. Becher, M. J. Mark, F. Wächtler, L. Santos, and F. Ferlaino, Observation of roton mode population in a dipolar quantum gas, Nat. Phys. **14**, 442 (2018).
[29] P. B. Blakie, D. Baillie, L. Chomaz, and F. Ferlaino, Supersolidity in an elongated dipolar condensate, Phys. Rev. Research **2**, 043318 (2020).
[30] G. Biagioni, N. Antolini, A. Alaa, M. Modugno, A. Fioretti, C. Gabbanini, L. Tanzi, and G. Modugno, Dimensional Crossover in the Superfluid-Supersolid Quantum Phase Transition, Phys. Rev. X **12**, 021019 (2016).
[31] J. Hertkorn, J.-N. Schmidt, M. Guo, F. Böttcher, K. S. H. Ng, S. D. Graham, P. Uerlings, H. P. Büchler, T. Langen, M. Zwierlein, and T. Pfau, Supersolidity in Two-Dimensional Trapped Dipolar Droplet Arrays, Phys. Rev. Lett. **127**, 155301 (2021).
[32] T. Macrì, F. Maucher, F. Cinti, and T. Pohl, Elementary excitations of ultracold soft-core bosons across the superfluid-supersolid phase transition, Phys. Rev. A **87**, 061602 (R) (2013).
[33] N. Henkel, R. Nath, and T. Pohl, Three-Dimensional Roton Excitations and Supersolid Formation in Rydberg-Excited Bose-Einstein Condensates, Phys. Rev. Lett. **104**, 195302 (2010).
[34] M. Sohmen, C. Politi, L. Klaus, L. Chomaz, M. J. Mark, M. A. Norcia, and F. Ferlaino, Birth, Life, and Death of a Dipolar Supersolid, Phys. Rev. Lett. **126**, 233401 (2021).
[35] F. Wächtler and L. Santos, Quantum filaments in dipolar Bose-Einstein condensates, Phys. Rev. A **93**, 061603(R) (2016).
[36] R. N. Bisset, R. M. Wilson, D. Baillie, and P. B. Blakie, Ground-state phase diagram of a dipolar condensate with quantum fluctuations, Phys. Rev. A **94**, 033619 (2016).
[37] I. Ferrier-Barbut, H. Kadau, M. Schmitt, M. Wenzel, and T. Pfau, Observation of Quantum Droplets in a Strongly Dipolar Bose Gas, Phys. Rev. Lett. **116**, 215301 (2016).
[38] L. Chomaz, S. Baier, D. Petter, M. J. Mark, F. Wächtler, L. Santos, and F. Ferlaino, Quantum-Fluctuation-Driven Crossover from a Dilute Bose-Einstein Condensate to a Macrodroplet in a Dipolar Quantum Fluid, Phys. Rev. X **6**, 041039 (2016).
[39] T. Lahaye, C. Menotti, L. Santos, M. Lewenstein, and T. Pfau, The physics of dipolar bosonic quantum gases, Rep. Prog. Phys. **72**, 126401 (2009).
[40] See Supplemental Material http://link.aps.org/supplemental/10.1103/PhysRevLett.128.195302 for a detailed analysis of our finite-temperature theory parameters and discussion of the excitations of a two-dimensional supersolid, which includes additional Refs. [41–54].
[41] S. Ronen, D. C. E. Bortolotti, and J. L. Bohn, Bogoliubov modes of a dipolar condensate in a cylindrical trap, Phys. Rev. A **74**, 013623 (2006).
[42] A. R. P. Lima and A. Pelster, Quantum fluctuations in dipolar bose gases, Phys. Rev. A **84**, 041604(R) (2011).
[43] S. P. Cockburn and N. P. Proukakis, *Ab initio* methods for finite-temperature two-dimensional bose gases, Phys. Rev. A **86**, 033610 (2012).
[44] S. Eckel, A. Kumar, T. Jacobson, I. B. Spielman, and G. K. Campbell, A Rapidly Expanding Bose-Einstein Condensate: An Expanding Universe in the Lab, Phys. Rev. X **8**, 021021 (2018).
[45] M. Ota, F. Larcher, F. Dalfovo, L. Pitaevskii, N. P. Proukakis, and S. Stringari, Collisionless Sound in a Uniform Two-Dimensional Bose Gas, Phys. Rev. Lett. **121**, 145302 (2018).
[46] T. Bland, Q. Marolleau, P. Comaron, B. Malomed, and N. Proukakis, Persistent current formation in double-ring geometries, J. Phys. B **53**, 115301 (2020).
[47] S. De, D. L. Campbell, R. M. Price, A. Putra, B. M. Anderson, and I. B. Spielman, Quenched binary Bose-Einstein condensates: Spin-domain formation and coarsening, Phys. Rev. A **89**, 033631 (2014).
[48] C. W. Gardiner and M. J. Davis, The stochastic Gross-Pitaevskii equation:II, J. Phys. B **36**, 4731 (2003).
[49] S. J. Rooney, P. B. Blakie, and A. S. Bradley, Stochastic projected Gross-Pitaevskii equation, Phys. Rev. A **86**, 053634 (2012).
[50] R. Kubo, The fluctuation-dissipation theorem, Rep. Prog. Phys. **29**, 255 (1966).
[51] E. B. Linscott and P. B. Blakie, Thermally activated local collapse of a flattened dipolar condensate, Phys. Rev. A **90**, 053605 (2014).
[52] D. Petter, A. Patscheider, G. Natale, M. J. Mark, M. A. Baranov, R. van Bijnen, S. M. Roccuzzo, A. Recati, B. Blakie, D. Baillie, L. Chomaz, and F. Ferlaino, Bragg scattering of an ultracold dipolar gas across the phase transition from Bose-Einstein condensate to supersolid in the free-particle regime, Phys. Rev. A **104**, L011302 (2021).
[53] E. Poli, T. Bland, C. Politi, L. Klaus, M. A. Norcia, F. Ferlaino, R. N. Bisset, and L. Santos, Maintaining

supersolidity in one and two dimensions, Phys. Rev. A **104**, 063307 (2021).
[54] J. Goldstone, Field theories with superconductor solutions, Nuovo Cimento (1955–1965) **19**, 154 (1961).
[55] This method has been applied previously in a quasi-two-dimensional setting without quantum fluctuations [51].
[56] P. Blakie, A. Bradley, M. Davis, R. Ballagh, and C. Gardiner, Dynamics and statistical mechanics of ultra-cold Bose gases using c-field techniques, Adv. Phys. **57**, 363 (2008).
[57] S. J. Rooney, T. W. Neely, B. P. Anderson, and A. S. Bradley, Persistent-current formation in a high-temperature Bose-Einstein condensate: An experimental test for classical-field theory, Phys. Rev. A **88**, 063620 (2013).
[58] R. G. McDonald, P. S. Barnett, F. Atayee, and A. S. Bradley, Dynamics of hot Bose-Einstein condensates: Stochastic ehrenfest relations for number and energy damping, SciPost Phys. **8**, 029 (2020).
[59] Our initial state is $\psi(\mathbf{r},0)=\psi_0(\mathbf{r})+\sum_n' \alpha_n\phi_n(\mathbf{r})$, where ϕ_n are the single-particle states, α_n is a complex Gaussian random variable with $\langle|\alpha_n|^2\rangle=(e^{\epsilon_n/k_BT}-1)^{-1}+\frac{1}{2}$, and the sum is restricted to modes with $\epsilon_n\leq 2k_BT$, with $T=30$ nK.
[60] C. N. Weiler, T. W. Neely, D. R. Scherer, A. S. Bradley, M. J. Davis, and B. P. Anderson, Spontaneous vortices in the formation of Bose-Einstein condensates, Nature (London) **455**, 948 (2008).
[61] I.-K. Liu, S. Donadello, G. Lamporesi, G. Ferrari, S.-C. Gou, F. Dalfovo, and N. Proukakis, Dynamical equilibration across a quenched phase transition in a trapped quantum gas, Commun. Phys. **1**, 1 (2018).
[62] F. Maucher, T. Pohl, S. Skupin, and W. Krolikowski, Self-Organization of Light in Optical Media with Competing Nonlinearities, Phys. Rev. Lett. **116**, 163902 (2016).
[63] F. Zambelli, L. Pitaevskii, D. M. Stamper-Kurn, and S. Stringari, Dynamic structure factor and momentum distribution of a trapped bose gas, Phys. Rev. A **61**, 063608 (2000).
[64] P. B. Blakie, R. J. Ballagh, and C. W. Gardiner, Theory of coherent bragg spectroscopy of a trapped Bose-Einstein condensate, Phys. Rev. A **65**, 033602 (2002).
[65] P. B. Blakie, D. Baillie, and R. N. Bisset, Roton spectroscopy in a harmonically trapped dipolar Bose-Einstein condensate, Phys. Rev. A **86**, 021604(R) (2012).
[66] S. Ronen, D. C. E. Bortolotti, and J. L. Bohn, Radial and Angular Rotons in Trapped Dipolar Gases, Phys. Rev. Lett. **98**, 030406 (2007).
[67] M. Jona-Lasinio, K. Łakomy, and L. Santos, Roton confinement in trapped dipolar Bose-Einstein condensates, Phys. Rev. A **88**, 013619 (2013).
[68] R. N. Bisset, D. Baillie, and P. B. Blakie, Roton excitations in a trapped dipolar Bose-Einstein condensate, Phys. Rev. A **88**, 043606 (2013).
[69] We measure phase coherence as $C^p=1-(2/\pi)\int_{\mathcal{C}} dxdy|\psi(x,y)|^2|\theta(x,y)-\beta|/\int_{\mathcal{C}} dxdy|\psi(x,y)|^2$, where $\theta(x,y)$ is the phase of $\psi(x,y)$ in the $z=0$ plane and β is a fitting parameter to maximize C^p at each time. The integration region $\mathcal{C}$ encompasses the droplets.
[70] Relative to the crystal maturation time, each quench ramp ended at 5, −13, and −90 ms for the linear interaction quench, pancake interaction quench, and pancake temperature quench, respectively. Note that evaporative cooling continues after the $\{\mu,T\}$ quench ends, taking approximately a further 100 ms until the classical field modes have equilibrated with the high-energy modes [40].
[71] The density overlap is given by $C^d=\int d^3\mathbf{x}n(\mathbf{x}-\mathbf{x}_0,\phi_0,t)n_{\mathrm{GS}}/\int d^3\mathbf{x}n_{\mathrm{GS}}^2$, with the ground state density and time-dependent density, respectively, normalized as $\int d^3\mathbf{x}n_{\mathrm{GS}}=\int d^3\mathbf{x}n(\mathbf{x}-\mathbf{x}_0,\phi_0,t)=1$. The optimization parameters $\mathbf{x}_0$ and ϕ_0 are translations and a rotation, respectively, applied to the wave function to maximize C^d.